JACS
JOURNAL OF THE AMERICAN CHEMICAL SOCIETY
pubs.acs.org/JACS
Article

Formation and Evolution of $H_2C_3O^{+\bullet}$ Radical Cations: A Computational and Matrix Isolation Study

Pavel V. Zasimov, Daniil A. Tyurin, Sergey V. Ryazantsev, and Vladimir I. Feldman*

Cite This: J. Am. Chem. Soc. 2022, 144, 8115−8128
Read Online

ABSTRACT: The family of isomeric $H_2C_3O^{+\bullet}$ radical cations is of great interest for physical organic chemistry and chemistry occurring in extraterrestrial media. In this work, we have experimentally examined a unique synthetic route to the generation of $H_2C_3O^{+\bullet}$ from the $C_2H_2\cdots CO$ intermolecular complex and also considered the relative stability and monomolecular transformations of the $H_2C_3O^{+\bullet}$ isomers through high-level *ab initio* calculations. The structures, energetics, harmonic frequencies, hyperfine coupling constants, and isomerization pathways for several of the most important $H_2C_3O^{+\bullet}$ isomers were calculated at the UCCSD(T) level of theory. The complementary FTIR and EPR studies in argon matrices at 5 K have demonstrated that the ionized $C_2H_2\cdots CO$ complex transforms into the *E*-$HCCHCO^{+\bullet}$ isomer, and this latter species is supposed to be the key intermediate in further chemical transformations, providing a remarkable piece of evidence for kinetic control in low-temperature chemistry. Photolysis of this species at λ = 410−465 nm results in its transformation to the thermodynamically most stable $H_2CCCO^{+\bullet}$ isomer. Possible implications of the results and potentiality of the proposed synthetic strategy to the preparation of highly reactive organic radical cations are discussed.

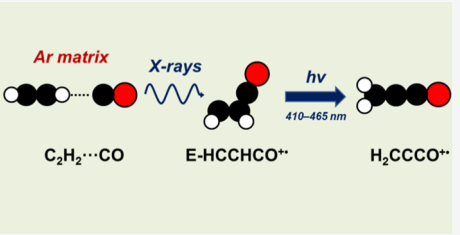

INTRODUCTION

Organic radical cations are known to be the key reactive intermediates in a wide variety of chemical processes, from interstellar and atmospheric chemistry to organic synthesis and photocatalysis.[1−10] In particular, small aliphatic species of this kind were the focus of many experimental and theoretical studies. Experimental information on intrinsic stability, thermochemistry, and possible monomolecular transformation pathways of such cations in the gas phase mostly comes from mass spectrometry and photoelectron spectroscopy,[11−15] whereas the detailed data on electronic and molecular structure, reaction kinetics, and environment effects could be extracted from the spectroscopic studies in the condensed phase.[16] However, many small radical cations (both hydrocarbon and heteroatomic) exhibit extremely high reactivity under ambient conditions, so they could be directly studied in the condensed phases only using ultrafast spectroscopy in the picosecond or even femtosecond time scale.[17,18] In this time window, usually the only available spectroscopic detection method is electronic absorption spectroscopy, which is superior for kinetic studies but often does not allow unambiguous structural identification and interpretation of the reaction pathways to be compared with theoretical predictions. The matrix isolation technique provides a very effective (and sometimes unique) way to overcome these limitations. In fact, this approach combines the advantages of low external perturbation (important for comparison with theory) and a virtually infinite lifetime of the studied species, which makes it possible to apply a variety of highly informative spectroscopic methods.[19−23] While the most common detection method in matrix isolation studies is Fourier transform infrared (FTIR) spectroscopy, a combination with electron paramagnetic resonance (EPR) spectroscopy is very useful in the case of open-shell species.[23−28] It is worth noting, however, that the application of combined FTIR/EPR studies to radical cations is still very limited, mainly due to experimental complications.[23]

Typically, radical cations can be generated in matrices through electron detachment from the corresponding neutral molecules using UV light or ionizing radiation.[19,22,23,29−32] However, this approach can be hardly applied if the parent neutrals are unavailable or unstable, which is often the case for small heteroatomic cyclic and unsaturated molecules. Meanwhile, there is a potentially useful (and sometimes unique) *synthetic* route to produce radical cations based on ionization of trapped intermolecular complexes composed of simpler molecules followed by their in-cage reactions. Such a strategy can be used to prepare the target unusual (or even exotic) heteroatomic radical cations from the suitable combinations of common stable precursors (e.g., small hydrocarbons, CO, H_2O, HCN). It may provide invaluable insight into the chemical dynamics of ionized states involved in many

Received: January 15, 2022
Published: April 29, 2022

https://doi.org/10.1021/jacs.2c00295
J. Am. Chem. Soc. 2022, 144, 8115−8128

Table 1. Summary of the Previous Theoretical and Experimental Investigations of the $H_2C_3O^{+\bullet}$ Radical Cations

Isomer	Structural depiction	Symmetry	Computed relative energy, kcal mol^{-1}		Obtained in the gas phase	
			ref 42[a]	ref 43[b,c]	Yes/No	ref
$H_2CCCO^{+\bullet}$ (**I**) *linear*	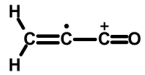	C_{2v}	0.5	0	Yes	42,44,45
bend	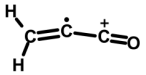	C_s	0.0		No	
c-$H_2C_3O^{+\bullet}$ (**II**)	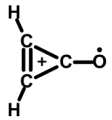	C_{2v}	27.2	15	Yes	46
$HCCCHO^{+\bullet}$ (**III**)	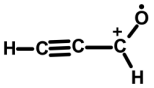	C_s	57.6	37	Yes	47–49
E-$HCCHCO^{+\bullet}$ (**IVa**)	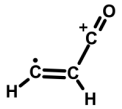	C_s	5.0	5		
					Yes[e]	42
Z-$HCCHCO^{+\bullet}$ (**IVb**)	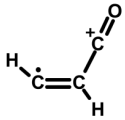	C_s	7.9	6		
$HCCCOH^{+\bullet}$ (**V**) *trans*	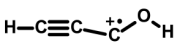	C_s	34.6		No	
				30[d]		
cis	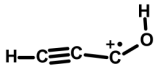	C_s	36.8		No	

[a]CI/6-31G**//HF/3-21G level of theory. [b]CBS-APNO level of theory. [c]Computed barriers for **IVa** → **IVb**, **IVa** → **II**, and **III** → **V** transformations are 7, 16, and 68 kcal mol^{-1}, respectively (see ref 43). [d]The exact molecular structure was not provided (see ref 43). [e]These isomers were not distinguished in the experiment (see ref 42).

processes both in the gas and in the condensed phases, which will allow reliable comparison with theory. It should be noted that, unlike the reactions of neutral radical−molecule complexes (see, for example, refs 33−35), the structure and chemical dynamics of charged open-shell species produced by ionization of complexes in matrices is poorly studied from both experimental and theoretical points of view. We may note that the studies of the radiation-induced evolution of complexes are particularly useful for modeling cold astrochemical processes occurring within the "building blocks" (recent examples may be found in refs 33 and 36−38). Most probably, this evolution taking place both in matrices and in mixed ices[39−41] includes the formation of complex radical cations as intermediates; however, direct pieces of evidence on this hidden stage are quite limited due to the rapid recombination of primary cations with electrons or their secondary reactions. Thus, efforts should be made to elaborate the way to isolate and identify the primary ionic species resulting from the complexes.

In this work, we are focusing on the preparation and characterization of the $H_2C_3O^{+\bullet}$ radical cations, which attract considerable attention as potentially important species in astrochemistry, physical organic chemistry, and mass spectrometry.[42−54] In particular, it was suggested[50,51] that the $H_2C_3O^{+\bullet}$ radical cations may be formed in the interstellar media (ISM) by the radiative association of $C_2H_2^{+\bullet}$ and CO and be an important source of interstellar C_3O. Based on the measured rate coefficients and product distributions of the $H_2C_3O^{+\bullet}$ radical cation reactions with main interstellar constituents, Petrie et al.[52,53] supposed a relatively long cloud lifetime for the $H_2C_3O^{+\bullet}$ radical cation. In addition, an efficient formation of more complex molecular ions was observed[52,53] as the result of several association reactions. Considering general chemical aspects, we may note that the family of the $H_2C_3O^{+\bullet}$ isomers represents a very interesting (and somewhat unique) example of small heteroatomic species with remarkable structural variability, which can be explicitly studied by computational methods at a high level of theory for direct comparison with experiment, and it may provide a sort of benchmark for modern physical organic chemistry.

The available literature data[42−49] on the theoretical and experimental investigation of the $H_2C_3O^{+\bullet}$ radical cation family are summarized in Table 1.

It should be stressed that we are unaware of any spectroscopic studies on the structure and reaction pathways of the $H_2C_3O^{+\bullet}$ radical cations in condensed phases. In search of a suitable complex precursor for the radical cations of this family in the frame of the synthetic strategy outlined above, we have considered a C_2H_2/CO system, which is supposed to play a very important role in ice astrochemistry.[55−57] Indeed, the formal stoichiometry of the C_2H_2···CO complex corresponds to the H_2C_3O formula. Furthermore, the reaction between $C_2H_2^{+\bullet}$ and CO was suggested as a possible way for the formation of the $H_2C_3O^{+\bullet}$ radical cation in the ISM.[50−53] In our recent study we demonstrated that the 1:1 C_2H_2···CO

https://doi.org/10.1021/jacs.2c00295
J. Am. Chem. Soc. 2022, 144, 8115−8128

intermolecular complex could be effectively stabilized in an Ar matrix by condensation of the C_2H_2/CO/Ar gaseous mixtures, and its X-ray irradiation at 5 K leads to the predominant formation of a number of synthetic produces containing a C_3O moiety.[58] Moreover, intermediate formation of the primary $H_2C_3O^{+\bullet}$ radical cation was tentatively suggested on the basis of preliminary spectroscopic findings.

In this work, we report the results of the first comprehensive theoretical and experimental study on the $H_2C_3O^{+\bullet}$ radical cations produced from the $C_2H_2\cdots CO$ complex isolated in an argon matrix, which is based on a combination of FTIR and EPR spectroscopy and high-level *ab initio* calculations.

COMPUTATIONAL AND EXPERIMENTAL DETAILS

Computational Details. All the calculations were performed with the Priroda 04 computer code.[59] Molecular geometries were fully optimized (tolerance of gradient is 10^{-6} au) at the valence correlated spin unrestricted UCCSD(T) level of theory.[60] The CCSD(T) level of theory was used to calculate closed-shell species. The augmented valence correlation consistent basis sets of type L2a_3, L3a_3, and L4a_3 were used.[61] These basis sets are analogous to the aug-cc-pVTZ, aug-cc-pVQZ, and aug-cc-pV5Z basis sets,[62−66] respectively, but include a larger number of primitive Gaussian functions. The comparative scheme of basis function contraction for LXa_3 and aug-cc-pVXZ basis sets (X − integer) is given in the Supporting Information (Table S1 of the SI). As shown previously,[67−69] the application of L2a_3 and L3a_3 basis sets provides good accuracy at a reasonable computational cost, and it was successfully used for the description of intermolecular complexes. The type of stationary points on a potential energy surface (PES) was checked by vibrational analysis at the UCCSD(T)/L2a_3 level of theory. The hyperfine coupling (HFC) tensors were evaluated from the spin density based on electric field gradient tensors at nuclear positions using the point nucleus model at the UCCSD(T)/L3a_3//UCCSD(T)/L3a_3 level of theory. Harmonic vibrational frequencies and IR intensities were calculated at the UCCSD(T)/L2a_3//UCCSD(T)/L2a_3 level of theory. IR intensities were calculated at the UCCSD(T)/L2a_3//UCCSD(T)/L2a_3 level of theory. The spin density distributions based on the UCCSD(T) natural orbital have been visualized using the Molden program.[70,71] The NON and MRI diagnostics[72] were applied to clarify the applicability of a single reference coupled cluster theory to the studied systems. In addition, the generalized atomic polar tensor (GAPT) atomic charges[73] were also computed for the investigated $H_2C_3O^{+\bullet}$ isomers and were used in order to evaluate the charge distribution in the investigated $H_2C_3O^{+\bullet}$ radical cations.

Extrapolation of energy to the complete basis set (CBS) limit was performed using the following formulas:[61]

$$E_{\infty}^{(\mathrm{CCSD})} = E_{x}^{(\mathrm{CCSD})} + \frac{(E_{x}^{(\mathrm{CCSD})} - E_{x-1}^{(\mathrm{CCSD})})}{\left(1 + \frac{1}{x+1/2}\right)^{3} - 1}$$

$$E_{\infty}^{(T)} = E_{x}^{(T)} + \frac{(E_{x}^{(T)} - E_{x-1}^{(T)})}{\left(1 + \frac{1}{x+1/2}\right)^{4} - 1}$$

$$E_{\infty}^{\mathrm{CCSD}(T)} = E_{x}^{\mathrm{HF}} + E_{\infty}^{(\mathrm{CCSD})} + E_{\infty}^{(T)}$$

where E_{∞} is extrapolated to CBS energy, $E_{\infty}^{(\mathrm{CCSD})}$, $E_{x}^{(\mathrm{CCSD})}$, and $E_{x-1}^{(\mathrm{CCSD})}$ are CCSD correlation energies extrapolated to CBS and computed with L3a_3 and L2a_3 sets, respectively, $E_{\infty}^{(T)}$, $E_{x}^{(T)}$, and $E_{x-1}^{(T)}$ are triple corrections extrapolated to CBS and computed with L3a_3 and L2a_3 sets, respectively, and E_{x}^{HF} is a Hartree−Fock energy, computed with the L4a_3 set. The extrapolation to CBS energies has been performed at UCCSD(T)/L3a_3 molecular geometries. The abbreviation UCCSD(T)/CBS is used for the extrapolation procedure described above. The zero-point vibrational energies (ZPVEs) have been calculated at the UCCSD(T)/L2a_3 level of theory.

For the 1:1 $(C_2H_2\cdots CO)^{+\bullet}$ and $C_2H_2\cdots CO$ complexes, the interaction energy was found as the difference between the UCCSD(T)/CBS energies of the complex and the monomers taking into account ZPVE correction.

Experimental Details. Acetylene ($^{12}C_2H_2$, 99.6%, SIAD; $^{13}C_2H_2$, 99.6% purity, 99% atom ^{13}C, Aldrich) and argon (Ar, 99.9995%, Voessen) were used without further purification. Carbon monoxide (CO, 98%, MGPZ) was purified by purging through two series-connected U-shaped tubes immersed in liquid nitrogen. Gaseous mixtures of C_2H_2/CO/Ar (the typical ratio is 1:1−3:1000) were prepared by the standard manometric procedure. Complementary experiments were carried out with sulfur hexafluoride (SF_6, 99.98%, Halogen) or Freon-11 ($CFCl_3$, 99.8%, Khimprom, Volgograd, Russia) as an electron scavenger (ES), and the typical C_2H_2/CO/ES/Ar mixture ratio was 1:3:1:1000. The choice of electron scavenger in FTIR and EPR matrix-isolation experiments was made taking into account minimum contamination of the observed spectra by the signals of the electron scavenger and its radiolysis products. For this reason, SF_6 was used in the FTIR experiments[74] and $CFCl_3$ was applied for the EPR studies.[23]

The matrix isolation experiments were carried out using two original closed-cycle helium cryostats based on SHI RDK-101E cryocoolers: one cryostat was utilized for FTIR experiments and the other one was applied in the EPR experiments. A detailed description of our experimental setup can be found elsewhere.[23] The cryostat chamber was evacuated to a level $<10^{-2}$ Pa before an experiment. Prepared gaseous mixtures were slowly deposited onto a cooled substrate (KBr plate in the FTIR experiments or sapphire rod in the EPR experiments). The temperature was controlled by a Lakeshore 325 controller connected to the calibrated Cernox-type temperature sensor and resistive heaters. The deposition temperature was chosen to obtain the samples with lower scattering of the IR beam (crucial for the FTIR matrix isolation experiments) containing a significant amount of the 1:1 $C_2H_2\cdots CO$ complex and to avoid the formation of higher aggregates. The temperature range of 13−18 K was found to be optimal for obtaining high amounts of intermolecular complexes. The thickness of the deposited samples in the FTIR experiments was controlled by monitoring interference fringes in the spectra. The deposition was stopped after reaching the appropriate film thickness (ca. 70−90 μm). In the EPR experiments, the thickness of the sample (controlled by visual inspection) was hundreds of μm.

The deposited matrix samples were slowly cooled to 5 K (minimal available temperature) and then irradiated with X-rays through an aluminum foil window (thickness of the foil was 45 μm) mounted in the cryostat from a 5BKhV-6(W) X-ray tube with a tungsten anode (45 kVp, anode current 80 mA, effective X-ray energy ca. 20 keV). The absorbed dose rate in the noble gas matrix samples was estimated in our earlier work[75] by using data from a calibrated Fricke dosimeter and Geant4 calculations of ratios of the absorbed dose rate in the 80 μm Ar matrix to that in the dosimeter. The value of the absorbed dose rates in an Ar matrix is 38.6 Gy s^{-1} (in the cryostat used for FTIR experiments). In the EPR experiments, the absorbed dose rate is roughly two times higher due to the smaller distance between a sample and the X-ray source window. The irradiation time varied from 1 to 88 min, so the samples were X-irradiated up to different absorbed doses (from 2 to 204 kGy, depending on irradiation time). Photolysis of the irradiated samples was performed using ARPL-STAR-3W LEDs (λ_D = 465 nm and λ_D = 410 nm).

The FTIR spectra of the samples were taken in the 6500−450 cm^{-1} range at 5 K using a Bruker Tensor II spectrometer equipped with a cooled MCT detector (resolution of 1 cm^{-1}, averaging by 144 scans). EPR spectra were recorded using an X-band (9.4 GHz) spectrometer with a high-frequency (100 kHz) magnetic field modulation and appropriate microwave power (from 5 to 138 μW). The initial models for fitting the EPR spectra were prepared manually utilizing the Bruker SIMFONIA[76] program with the computed HFC tensors (see Computational Details) and *g*-tensor of a free electron as starting parameters. Fitting of the initial simulation to the experimental data

https://doi.org/10.1021/jacs.2c00295
J. Am. Chem. Soc. 2022, 144, 8115−8128

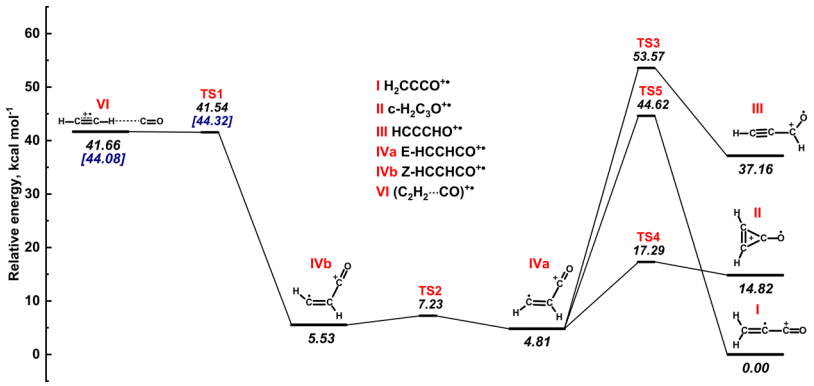

Figure 1. Relative energies of the investigated $H_2C_3O^{+\bullet}$ isomers calculated at the UCCSD(T)/CBS level (including the ZPVE correction calculated at the UCCSD(T)/L2a_3 level). ZPVE-uncorrected energies for the **VI** complex and **TS1** in kcal mol^{-1} relative to the ZPVE-uncorrected $H_2CCCO^{+\bullet}$ (**I**) minimum (see text for details) are provided in square brackets. Revealed reaction pathways are pointed out with black lines. The *ab initio* energies of the stationary points are given in kcal mol^{-1} relative to the ZPVE-corrected $H_2CCCO^{+\bullet}$ (**I**) minimum unless otherwise noted.

was made by means of the EasySpin[77] program. HFC tensors and *g*-tensors were treated as diagonal matrices, while the peak-to-peak line width was simulated in isotropic approximation using the Voight (convolution of Gaussian and Lorentzian curves) profile. The line width anisotropy was omitted in the simulation.

COMPUTATIONAL RESULTS

The previous theoretical and experimental data on the neutral $C_2H_2\cdots CO$ complex (see ref 78 and references therein) revealed that the thermodynamically favorable structure is a linear carbon-bonded HCCH···CO geometry of $C_{\infty v}$ symmetry, so we have examined this structure at the CCSD(T)/L3a_3 level (Figure S1 of the SI; Cartesian coordinates are provided in Table S2 of the SI). Ionization of the neutral HCCH···CO complex (vertical ionization energy (IE) 11.334 eV at the CBS level) leads to shrinking of the geometry of the charged linear $(HCCH\cdots CO)^{+\bullet}$ complex ($C_{\infty v}$ symmetry, designated hereafter as isomer **VI** of $H_2C_3O^{+\bullet}$) and some elongation of C≡C and C−H bonds (Figure S1 of the SI; Cartesian coordinates are provided in Table S2 of the SI). The adiabatic IE of the $C_2H_2\cdots CO$ complex was found to be 11.206 eV at the CBS level (11.204 eV at the CBS+ZPVE level), and the carbon-bonded geometry is retained due to a rather small relaxation energy of 2.95 kcal mol^{-1} of the charged complex after ionization. The UCCSD(T)/CBS adiabatic IE of the acetylene molecule is 11.427 eV (11.407 eV at the CBS+ZPVE level) and agrees well with the PFI-ZEKE experimental data (11.40078 ± 0.00006 eV),[79] while that of the carbon monoxide molecule is 14.051 eV (14.059 eV at the CBS +ZPVE level), also in good agreement with the experimental value of 14.0142 ± 0.0003 eV obtained from the REMPI mass spectroscopy study.[80] It is worth noting that the theoretical value of the adiabatic IE of the complex is close to that of acetylene, which may indicate that the positive charge is mostly located on the acetylene molecule. According to the CBS calculations taking into account the ZPVE correction, complex $(C_2H_2\cdots CO)^{+\bullet}$ (**VI**) lies 5.23 kcal mol^{-1} lower in energy than the isolated $C_2H_2^{+\bullet}$ and CO monomers, while the neutral precursor complex $C_2H_2\cdots CO$ is only 0.53 kcal mol^{-1} lower in energy than the isolated C_2H_2 and CO; that is, ionization, results in stronger binding between the components. A rather big positive value of complex formation energy implies that the complex should be thermodynamically stable with respect to decomposition onto $C_2H_2^{+\bullet}$ and CO species under the matrix isolation condition.

Analysis of the $H_2C_3O^{+\bullet}$ PES at the UCCSD(T)/CBS//UCCSD(T)/L3a_3 level of theory revealed the existence of the energy minima corresponding to the **I** ($H_2CCCO^{+\bullet}$), **II** (c-$H_2C_3O^{+\bullet}$), **III** ($HCCCHO^{+\bullet}$), **IVa** (*E*-$HCCHCO^{+\bullet}$), and **IVb** (*Z*-$HCCHCO^{+\bullet}$) structures of $H_2C_3O^{+\bullet}$. In agreement with previous reports,[42,43] our computational results demonstrate that the $H_2CCCO^{+\bullet}$ (**I**) species is the most thermodynamically stable structure within the whole $H_2C_3O^{+\bullet}$ family. Thus, the $H_2C_3O^{+\bullet}$ PES is analyzed with respect to the $H_2CCCO^{+\bullet}$ energy. The isomer **II** (cyclopropenone radical cation) has C_{2v} symmetry. The isomer **III** (propynal radical cation) has a C_s symmetry, and it was found to be the least stable structure among the investigated $H_2C_3O^{+\bullet}$ radical cations, which also fully agrees with the previous reports.[42,43] We have also identified two minima (both of C_s symmetry) corresponding to the **IVa** (*E*-$HCCHCO^{+\bullet}$) and **IVb** (*Z*-$HCCHCO^{+\bullet}$) isomers. The optimized geometries and relative energies of the computed PES minima are presented in Figure S2 of the SI; Cartesian coordinates and energies are presented in Tables S2 and S3 of the SI. The spin-squared (S^2), T_1, NON, and MRI diagnostics for the investigated $H_2C_3O^{+\bullet}$ isomers are provided in Table S4. The results of NON and MRI diagnostics[72] definitely show the single-reference nature of the coupled cluster wave functions of all studied radical cations. The single-reference nature of the coupled cluster wave functions indicates that the coupled cluster procedure effectively reduces the spin contamination, which comes from admixing higher multiplet states to the reference unrestricted Hartee−Fock wave function.[81,82] The charge distribution analysis performed in our study (based on the computed GAPT atomic charges; see Table S2 of the SI) confirms the Lewis structure depictions reported earlier for the **I**, **II**, **IVa**, and **IVb** isomers of $H_2C_3O^{+\bullet}$.[42,43] As to isomer **III**, our results show that charge is located at carbon rather than the oxygen atom (as implied in earlier reports[42,43]), which indicates the separation of charge and spin.

All the studied isomers are stable with respect to decomposition onto the $C_2H_2^{+\bullet}$ and CO species (the total energy for this pair was computed to be 46.89 kcal mol^{-1}). Additionally, we calculated the total energy of the separated fragments HC_3O^+ and $H^\bullet$, which was found to be 48.03 kcal mol^{-1}; that is, it exceeds the energy of the $(C_2H_2\cdots CO)^{+\bullet}$

https://doi.org/10.1021/jacs.2c00295
J. Am. Chem. Soc. 2022, 144, 8115−8128

Table 2. Harmonic Frequencies and IR Intensities (km mol^{-1}, Provided in Parentheses) for the Studied $H_2C_3O^{+\bullet}$ Radical Cation Isomers Calculated at the UCCSD(T)/L2a_3 Level

	harmonic frequency, cm^{-1}					
mode number	$H_2CCCO^{+\bullet}$ (I)	c-$H_2C_3O^{+\bullet}$ (II)	$HCCCHO^{+\bullet}$ (III)	*E*-$HCCHCO^{+\bullet}$ (IVa)	*Z*-$HCCHCO^{+\bullet}$ (IVb)	$(C_2H_2\cdots CO)^{+\bullet}$ (VI)
1	57.4 (3.3)	347.1 (0.5)	158.8 (6.1)	219.9 (0.9)	212.1 (5.2)	66.3 (4.3)
2	182.2 (1.0)	484.1 (2.8)	215.3 (30.0)	416.2 (4.0)	428.7 (8.2)	93.1 (1.1)
3	422.0 (12.8)	725.8 (12.9)	448.4 (19.5)	593.9 (21.2)	579.8 (1.4)	139.8 (67.3)
4	574.2 (25.3)	775.3 (70.7)	730.5 (32.2)	690.3 (74.5)	716.3 (22.6)	180.8 (9.9)
5	878.6 (0.0)	806.7 (0.0)	833.5 (14.5)	757.5 (16.4)	787.9 (56.4)	190.4 (1.2)
6	899.6 (0.9)	806.8 (15.5)	926.4 (0.6)	885.5 (0.5)	886.1 (52.7)	605.4 (20.1)
7	1019.8 (27.1)	949.0 (0.8)	999.3 (48.8)	999.1 (14.6)	963.9 (1.2)	770.0 (15.3)
8	1394.0 (33.6)	977.1 (25.7)	1178.2 (21.9)	1224.1 (8.1)	1234.3 (4.6)	853.8 (66.2)
9	1821.0 (13.5)	1510.2 (0.0)	1521.4 (183.9)	1592.0 (136.6)	1576.9 (108.5)	883.1 (1.4)
10	2287.0 (701.0)	1769.4 (0.1)	2226.8 (467.9)	2317.2 (317.7)	2300.2 (308.8)	1837.4 (101.3)
11	3067.8 (74.6)	3203.2 (177.4)	2926.7 (110.9)	3113.8 (66.6)	3161.0 (81.1)	2211.7 (25.5)
12	3164.3 (61.1)	3255.1 (87.1)	3396.1 (79.6)	3253.6 (67.2)	3254.6 (47.9)	3132.9 (1723.6)
13						3305.0 (882.7)

Table 3. HFC Tensors Principal Values (mT) for the $H_2C_3O^{+\bullet}$ Radical Cation Isomers Calculated at the UCCSD(T)/L3a_3 Level[a]

	$H_2CCCO^{+\bullet}$ (I)		c-$H_2C_3O^{+\bullet}$ (II)		$HCCCHO^{+\bullet}$ (III)		*E*-$HCCHCO^{+\bullet}$ (IVa)		*Z*-$HCCHCO^{+\bullet}$ (IVb)		$(C_2H_2\cdots CO)^{+\bullet}$ (VI)	
	a_{iso}	a_1	a_{iso}	a_1	a_{iso}	a_1	a_{iso}	a_1	a_{iso}	a_1	a_{iso}	a_1
		a_2		a_2		a_2		a_2		a_2		a_2
nucleus		a_3		a_3		a_3		a_3		a_3		a_3
$^1H_1$	4.67	4.49	2.90	2.54	−0.36	−0.45	5.13	4.90	3.61	3.38	−1.74	−2.54
		4.53		2.77		−0.43		5.05		3.40		−1.88
		4.99		3.38		−0.19		5.43		4.04		−0.81
$^1H_2$	4.67	4.49	2.90	2.54	8.76	8.38	0.41	−0.86	0.11	−1.16	−1.78	−2.64
		4.53		2.77		8.56		0.14		−0.11		−1.91
		4.99		3.38		9.35		1.95		1.59		−0.79
$^{13}C_3$	−1.55	−1.79	2.32	1.57	1.19	1.11	−1.22	−1.72	0.63	0.24	−0.03	−2.12
		−1.47		1.64		1.14		−1.29		0.66		−1.44
		−1.38		3.76		1.31		−0.64		0.99		3.46
$^{13}C_4$	0.81	−1.22	2.32	1.57	3.55	3.18	11.13	8.20	12.71	9.83	−0.03	−2.18
		−1.15		1.64		3.26		8.66		10.28		−1.48
		4.79		3.76		4.22		16.54		18.02		3.57
$^{13}C_5$	−1.97	−2.36	−2.67	−3.28	−2.08	−2.64	2.76	2.60	4.83	4.65	−0.19	−0.20
		−1.96		−2.51		−1.90		2.69		4.67		−0.20
		−1.60		−2.22		−1.71		2.98		5.18		−0.17
$^{17}O_6$	−0.52	0.93	−1.45	2.04	−1.63	3.50	−0.15	−0.08	−0.28	−0.10	0.01	0.01
		0.84		1.62		2.85		−0.15		−0.19		0.01
		−3.32		−8.01		−11.24		−0.22		−0.54		0.01

[a]Order and numeration of nuclei are provided in Figure S2 of the SI.

complex by 6.37 kcal mol^{-1}. It implies that the dissociation of the $(C_2H_2\cdots CO)^{+\bullet}$ complex into HC_3O^+ and $H^\bullet$ species is a thermodynamically unfavorable process. Furthermore, according to our calculations, the decomposition of the **VI** complex into $C_3O^{+\bullet}$ and H_2 fragments is even less favorable because the total energy of $C_3O^{+\bullet}$ and H_2 exceeds the energy of the complex by 46.17 kcal mol^{-1}.

Further evolution of the $(C_2H_2\cdots CO)^{+\bullet}$ complex on the PES was found to result in the low energetic reaction sequence $(C_2H_2\cdots CO)^{+\bullet}$ (**VI**) → *Z*-$HCCHCO^{+\bullet}$ (**IVb**) → *E*-$HCCHCO^{+\bullet}$ (**IVa**) with CBS+ZPVE energies of 41.66, 5.53, and 4.81 kcal mol^{-1} for the **VI**, **IVb**, and **IVa** isomers, respectively (Figure 1). This transformation started through the low-energetic **TS1** barrier of 0.24 kcal mol^{-1} between **VI** and **IVb** species according to the UCCSD(T)/CBS calculations. The **VI** → **IVb** transformation barrier is practically negligible (if any). **TS1** was found to be only 0.24 kcal mol^{-1} higher in energy than the $(C_2H_2\cdots CO)^{+\bullet}$ complex at the UCCSD(T)/CBS level. The introduction of the ZPVE correction gives a negative value of −0.12 kcal mol^{-1} for the **VI** → **IVb** reaction barrier, which may arise due to small inaccuracies in the theory used (Figure 1). The transformation between **IVb** and **IVa** species occurs through the **TS2** barrier of 1.70 kcal mol^{-1}. A rather big energy gap (36.13 kcal mol^{-1}) between **VI** and **IVb** structures and a virtually absent transition state implies that the $(C_2H_2\cdots CO)^{+\bullet}$ complex is metastable toward a chemical condensation. One can consider several reaction pathways of the **IVa** molecule. The first one leads to the $HCCCHO^{+\bullet}$ (**III**) radical cation with a CBS+ZPVE energy of 37.16 kcal mol^{-1} through the **TS3** barrier of 48.76 kcal mol^{-1} between the **IVa** and **III** isomers. Another opportunity is the formation of a c-$H_2C_3O^{+\bullet}$ (**II**) isomer with the CBS+ZPVE

https://doi.org/10.1021/jacs.2c00295
J. Am. Chem. Soc. 2022, 144, 8115−8128

energy of 14.82 kcal mol^{-1} through the **TS4** barrier of 12.48 kcal mol^{-1} between the **IVa** and **II** isomers. Finally, there is a pathway leading to the $H_2CCCO^{+\bullet}$ (**I**) isomer through the **TS5** barrier of 39.81 kcal mol^{-1} between the **IVa** and **I** species. The optimized geometries, energies, and harmonic frequencies related to the **TS1**−**TS5** are provided in Tables S2, S3, S5, and Figure S3 of the SI.

We have also calculated harmonic frequencies and HFC tensors for the $H_2C_3O^{+\bullet}$ isomers and the $(C_2H_2\cdots CO)^{+\bullet}$ complex. The results are given in Tables 2 and 3 (harmonic frequencies for several carbon-substituted isotopomers of the studied $H_2C_3O^{+\bullet}$ species are presented in Table S6 of the SI; vibrational modes assignment can be also found there). Considering these data, we may notice that the computed intensity of the C═O stretching mode (2287.0 cm^{-1}) of the most stable isomer **I** (propadienone radical cation) exceeds the intensities of all other vibrations of this molecule approximately by an order of magnitude. Hence, this feature should be easily observed in the IR spectra. The most intense absorption modes of the cyclopropenone radical cation (**II**) have calculated harmonic frequencies of 3203.2 and 3255.1 cm^{-1}, which correspond to antisymmetric and symmetric C−H stretching, respectively. Remarkably, this species (unlike all other isomers) has no intense absorptions corresponding to C═O stretching, and the CCO stretching predicted at 1769.4 cm^{-1} is almost inactive in the IR spectra. The $HCCHCO^{+\bullet}$ (**III**) radical cation has intense vibrational C═O, C≡C, and aldehyde C−H stretching modes (1521.4, 2226.8, and 2926.7 cm^{-1}, respectively). The most intense modes both of **IVa** and **IVb** species are C═O (2317.2 and 2300.2 cm^{-1}, respectively) and C═C stretching (1592.0 and 1576.9 cm^{-1}, respectively) while in the **VI** complex the antisymmetric and symmetric C−H stretching and symmetric C≡C stretching modes (3132.9, 3305.0, and 1837.4 cm^{-1}, respectively) of the acetylene are the most intense vibrations. One may note that the calculations clearly show lifting of the degeneracy (i.e., splitting) of the acetylene bending vibrations in the radical cation complex $(C_2H_2\cdots CO)^{+\bullet}$ (isomer **VI**), which means that this complex is subjected to a Renner−Teller distortion (similar to the acetylene radical cation $C_2H_2^{+\bullet}$).[83] Remarkably, the computed intensity of the C−H stretching modes in the complex increase strongly as compared to that in acetylene radical cation (see Table S6 of the SI).

Considering the HFC constants (see Table 3), one may notice that **I** and **II** isomers have two magnetically equivalent protons, and therefore these species should give a triplet spectral pattern of the EPR signal with an intense central component corresponding to $M_I = 0$. In contrast, the radical cations **III**, **IVa**, and **IVb** have two inequivalent protons, so one should expect a doublet of doublets with strongly different HFC splittings. We will address a more detailed discussion in the Experimental Results section.

EXPERIMENTAL RESULTS

FTIR Spectroscopic Studies. The C_2H_2/CO/Ar matrices deposited at 13−18 K contained a sufficient amount of matrix-isolated 1:1 $C_2H_2\cdots CO$ complexes (besides C_2H_2 and CO monomers as well as other aggregates), as evidenced by characteristic IR absorptions at 3281.5, 2143.1, 747.4, and 742.5 ($^{12}C_2H_2\cdots CO$) and 3274.4, 2143.1, 745.5, and 740.6 cm^{-1} ($^{13}C_2H_2\cdots CO$) described in our previous paper.[58] FTIR spectroscopy identification of the complex relied on comparison to gas-phase data and quantum chemical computations at the CCSD(T)/L3a_3 level of theory (predicted harmonic frequencies of $C_2H_2\cdots CO$, C_2H_2, and CO can be found in Table S7 of the SI). Irradiation of the C_2H_2/CO/Ar samples with X-rays results in decomposition of the $C_2H_2\cdots CO$ complexes and formation of new molecular species as described in detail in our previous paper.[58] According to these data, radiolysis of $C_2H_2\cdots CO$ yields C_3O (tricarbon monoxide), $HC_3O^{\bullet}$ (oxoprorynyl radical), HCCCHO (propynal), H_2CCCO (propadienone), and c-H_2C_3O (cyclopropenone).[58] In the present work we are focusing on the previously unidentified intermediate product of the radiation-induced evolution of the $C_2H_2\cdots CO$ complex manifested itself by a broadened IR absorption at 2265.6 (for $^{12}C_2H_2\cdots^{12}CO$) or 2263.7 cm^{-1} (in the case of $^{13}C_2H_2\cdots^{12}CO$). This spectral feature (denoted as **X** in our previous study[58]) was observed only in matrices containing both CO and C_2H_2 (presuming its origin from the $C_2H_2\cdots CO$ complex but not from C_2H_2 or CO), and it did not belong to any known C_3 product. This absorption appeared in the region of strongly blue-shifted CO vibrations and demonstrated rapid formation of the corresponding carrier at low conversions of the $C_2H_2\cdots CO$ complex (below 10%) followed by its gradual decay at a high absorbed dose. On the basis of such kinetic behavior, we had tentatively assigned the band in focus to some intermediate species (presumably cationic) arising directly from the $C_2H_2\cdots CO$ complex.[58] The idea that this unknown species might be a cation comes from the observation of the increased yield of C_2H^- in the C_2H_2/CO/Ar matrices (as compared to C_2H_2/Ar ones), while the yield of Ar_2H^+ had not been evidently affected by the presence of CO. To note, the Ar_2H^+ cations most probably originate from deprotonation of extremely acidic $H_2O^{+\bullet}$ radical cations (a small amount of water is a typical impurity in matrix-isolation experiments).[39]

In order to confirm the cationic nature of the species responsible for the above-mentioned absorption, we have performed the experiments with the electron scavenger added in the matrices. The FTIR spectra of the X-irradiated C_2H_2/CO/SF_6/Ar samples demonstrate a strong effect of the scavenger on the yields of the radiolysis products resulting from C_2H_2 and $C_2H_2\cdots CO$ (in additon to formation of the well-known products of the SF_6 radiolysis, mainly absorbing in the low-frequency region;[84] see Figure S4 of the SI. In particular, we have observed a noticeable increase (roughly up to three times) in the intensity of the absorption band at 2265.6 cm^{-1} (denoted as **A** in the present work) in the presence of SF_6, as compared to the scavenger-free samples, at a similar conversion degree of the parent complex (Figure 2). Analogous behavior was observed for the absorption at 2263.7 cm^{-1} (in the case of the system containing $^{13}C_2H_2$). Such behavior definitely supports the assignment of these absorptions to the C═O stretching mode. It should be stressed that the intensities of other unassigned absorption bands[58] did not increase in the presence of an electron scavenger. It is important to notice that the yields of all major neutral radiolysis products of the $C_2H_2\cdots CO$ complex except c-H_2C_3O (namely, C_3O, HCCCHO, and H_2CCCO) dramatically decrease in the presence of SF_6, and formation of these products demonstrates a well-defined induction period, which was not observed in the absence of scavenger (see Figure 3). In contrast, the yield of c-H_2C_3O species increases (see Figures 2 and 3).

As shown in Figure 4, the photolysis of the irradiated $^{12}C_2H_2$/CO/SF_6/Ar samples with blue or violet light (λ_D =

https://doi.org/10.1021/jacs.2c00295
J. Am. Chem. Soc. 2022, 144, 8115−8128

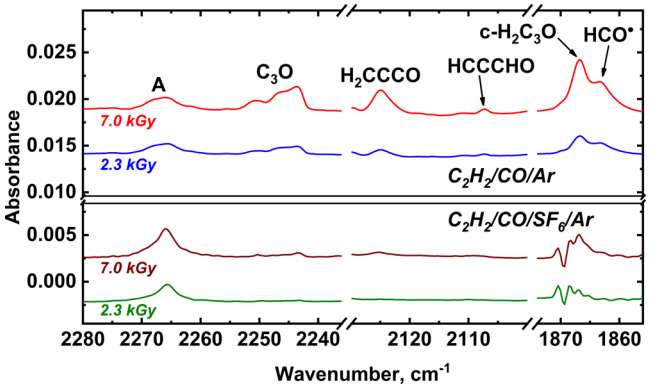

Figure 2. Difference FTIR spectra of the $^{12}C_2H_2$/CO/Ar (1:3:1000) irradiated samples (top panel) and $^{12}C_2H_2$/CO/SF_6/Ar (1:3:1:1000) irradiated samples (bottom panel) showing the effect of an electron scavenger (SF_6) addition on the C_3O, H_2CCCO, HCCCHO, and c-H_2C_3O signals and feature **A**. Absorptions in the bottom spectra at 1869.5 cm^{-1} are the effect of atmospheric water.

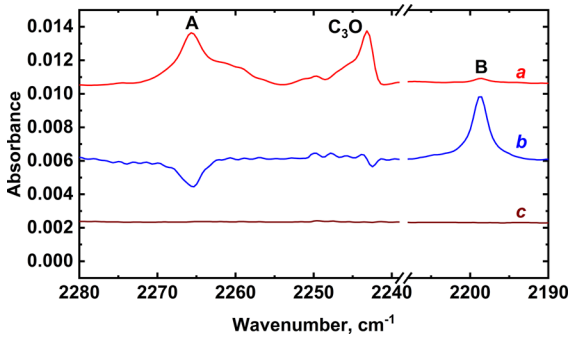

Figure 4. Difference FTIR spectra of the $^{12}C_2H_2$/CO/SF_6/Ar 1:3:1:1000 sample illustrating the effect of 20 min radiolysis (a), subsequent photolysis of the irradiated sample with λ_D = 465 nm light for 10 min (b), and standing of the irradiated and photolyzed sample for 20 min without photolysis (c).

465 or 410 nm) results in the decrease of the intensity of **A** and the appearance of the new feature with a maximum at 2198.6 cm^{-1} (denoted as **B** in the present work). In correlation with this result, the photoinduced decay of the band at 2263.7 cm^{-1} was accompanied by the growth of a new band at 2189.4 cm^{-1} in the experiments with ^{13}C-labeled acetylene. In fact, one could notice that a weak signal of **B** was observed already in the irradiated sample before photolysis. The intensity of the HCO• and Ar_2H^+ absorptions also significantly decreased as a result of photolysis, while the intensities of other bands in the IR spectrum were almost unaffected by photolysis.

The FTIR spectroscopic results clearly demonstrate that the absorption band denoted as **A** belongs to some cationic photosensitive species originating from the C_2H_2···CO complex. However, its identity and mechanism of phototransformations cannot be unequivocally established on the sole basis of these data, because only one absorption is observed for both parent species and product of photoreaction. Indeed, comparison with computational results (see Table 2) shows that the C═O stretching frequency for, at least, three isomers of the $H_2C_3O^{+\bullet}$ radical cation (**I**, **IVa**, and **IVb**) may be responsible for the experimentally observed feature at 2265.6 cm^{-1}, taking into account typical overestimation of the calculated frequencies for such vibrations due to neglect of anharmonicity and matrix effects. Thus, one needs additional arguments for identification.

EPR Spectroscopic Studies. While the IR spectroscopic results provide strong evidence on the cationic character of the intermediate in focus, the EPR spectroscopy may prove its radical nature and reveal the magnetic nuclei (protons), which is crucial for the assignment. In order to unambiguously identify the species formed in a complex system providing the maximum amount of intermediate in question, we have studied the paramagnetic products resulting from radiolysis of C_2H_2/Ar, C_2H_2/$CFCl_3$/Ar, C_2H_2/CO/Ar, and C_2H_2/CO/$CFCl_3$/Ar samples (we may note that CO itself is known to be radiation resistant in argon[85]). $CFCl_3$ was used as an electron scavenger in the EPR experiments. We should note that all the spectra of irradiated systems reveal a strong doublet with the large characteristic splitting of ca. 51 mT (see, for example, ref 86) due to trapped H• atoms produced from the radiolysis of acetylene[87] (and partially from water and other impurities). In addition, a very weak signal of the CH_3• (methyl) radical (a quartet with a splitting of ca. 2.3 mT; see, for example, ref 88)

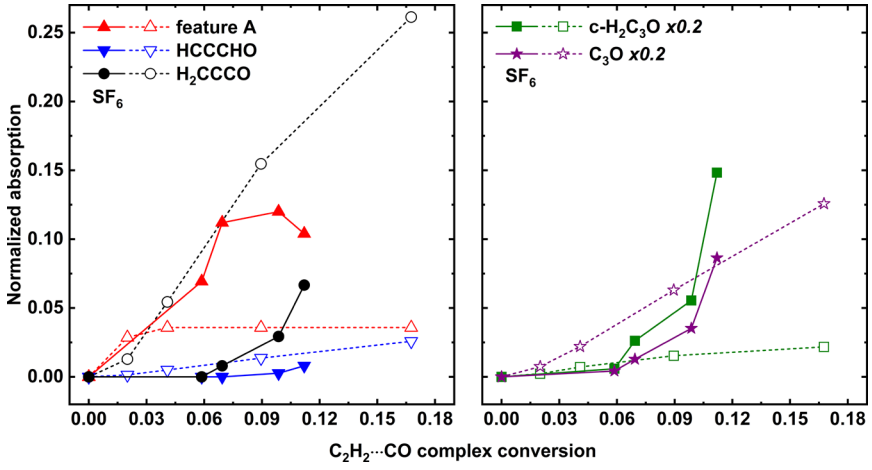

Figure 3. Accumulation profiles of the feature **A** and major neutral radiolysis products of the C_2H_2···CO complex (HCCCHO, H_2CCCO, c-H_2C_3O, and C_3O) in the presence (solid line, solid symbols) and the absence of an electron scavenger (dashed line, empty symbols). The corresponding absorption intensities were normalized to the parent complex absorption in the appropriate nonirradiated samples. Note that the signals of c-H_2C_3O and C_3O have been scaled for a better representation.

https://doi.org/10.1021/jacs.2c00295
J. Am. Chem. Soc. 2022, 144, 8115−8128

resulting from some common impurity is seen in all the studied systems (this is a typical situation in matrix isolation studies since this radical is easily observed, even if present in very low concentrations). In further consideration, we will refer to the central part of the spectra containing the signals of organic radicals produced from the studied system, as shown in Figure 5. In accordance with previously reported data,[89−91] the

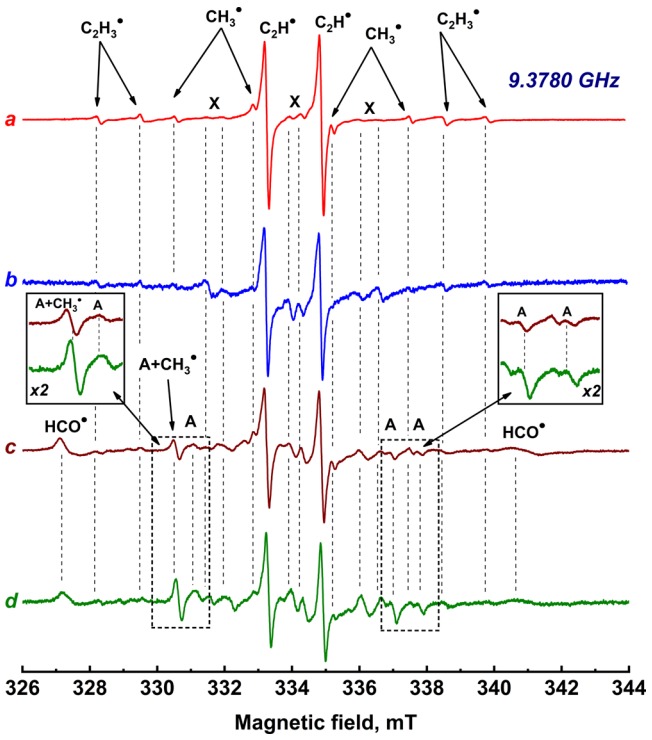

Figure 5. EPR spectra of the $^{12}C_2H_2$/Ar 1:1000 (*a*), $^{12}C_2H_2$/$CFCl_3$/Ar 1:1:1000 (*b*), $^{12}C_2H_2$/CO/Ar 1:3:1000 (*c*), and $^{12}C_2H_2$/CO/$CFCl_3$/Ar 1:3:1:1000 (*d*) irradiated samples. All the spectra were recorded at 5 K. Experimental microwave frequency is indicated in the top right corner. Acetylene-related species are marked with **X**; absorptions attributed to the $H_2C_3O^{+\bullet}$ radical cations are marked with **A** (see the text for details).

radiolysis of the C_2H_2/Ar binary system (Figure 5, *a*) reveals a strong signal of the $C_2H^\bullet$ (ethynyl) radical (slightly anisotropic doublet) as well as rather weak features of $C_2H_3^\bullet$ (vinyl) radical (a 2 × 2 × 2 multiplet due to the inequivalence of all the protons; some components are hidden due to overlapping with stronger signals from other species). The addition of the electron scavenger ($CFCl_3$) brings the enhancement of new weak signals, marked as **X** in Figure 5, which may be tentatively ascribed to acetylene radical cation ($C_2H_2^{+\bullet}$). To the best of our knowledge, the EPR spectrum of $C_2H_2^{+\bullet}$ has not been reported so far, and it may present a challenge for future experimental and theoretical studies, taking into account the structure and dynamics of this important species. However, the main goal of this work is the characterization of the $H_2C_3O^{+\bullet}$ radical cation, and here we refrain from speculations and treat the observed signals simply as belonging to an acetylene-related species **X**. The EPR spectrum of the X-irradiated $^{13}C_2H_2$/CO/$CFCl_3$/Ar 1:3:1:1000 sample is presented in Figure S5 of the SI).

On the basis of the results for the paramagnetic species originating from acetylene, we may approach the interpretation of the EPR spectra observed in the irradiated systems containing both acetylene and carbon monoxide (Figure 5, *c* and *d*). In addition to the above-considered signals, the spectrum of the C_2H_2/CO/Ar sample (Figure 5, *c*) reveals the presence of some extra lines. First, a well-known anisotropic doublet of the formyl ($HCO^\bullet$) radical appears at the spectral wings.[92] Second, and most important for the purpose of this study, we have found a number of new previously unreported features, which are not observed in the CO-free samples. Remarkably, the relative intensity of these lines increases significantly in the presence of an electron scavenger (Figure 5, *d*). In this respect, they demonstrate the same behavior as absorption **A** found in the IR spectra and are different from that of all other IR absorptions (see the previous subsection), so we also mark the corresponding lines in the EPR spectra as **A**. They should be reasonably ascribed to some radical cation resulting from the C_2H_2···CO complex. Further analysis will be based on consideration of the informative regions of the spectrum observed in the presence of an electron scavenger, which is shown in detail in Figure 6, *a*. We can see that this spectrum contains, at least, four lines denoted as **A** in the

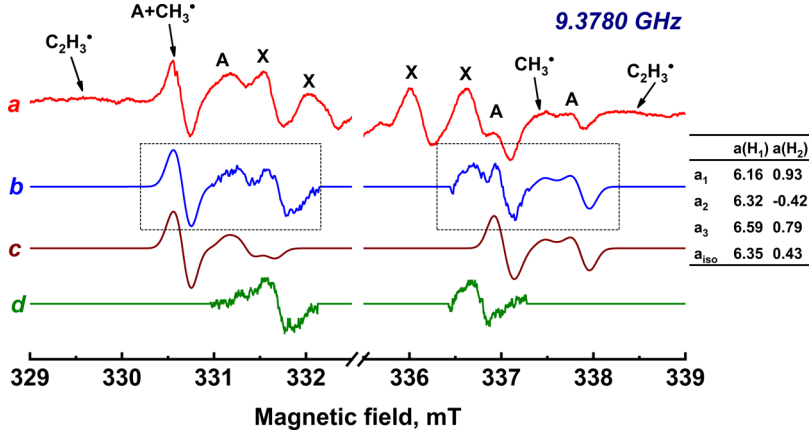

Figure 6. EPR spectra (recorded at 5 K) of the $^{12}C_2H_2$/CO/$CFCl_3$/Ar 1:3:1:1000 irradiated sample (*a*), the sum of the *c* and *d* spectra (*b*), simulation of the feature **A** (*c*), spectrum of the feature **X** (*d*). (See text for details.) The HFC constants (mT) extracted from the simulation of the feature **A** are provided in the right panel. Simulation areas are marked with dashed frames. Experimental microwave frequency is provided in the top right corner.

https://doi.org/10.1021/jacs.2c00295
J. Am. Chem. Soc. 2022, 144, 8115−8128

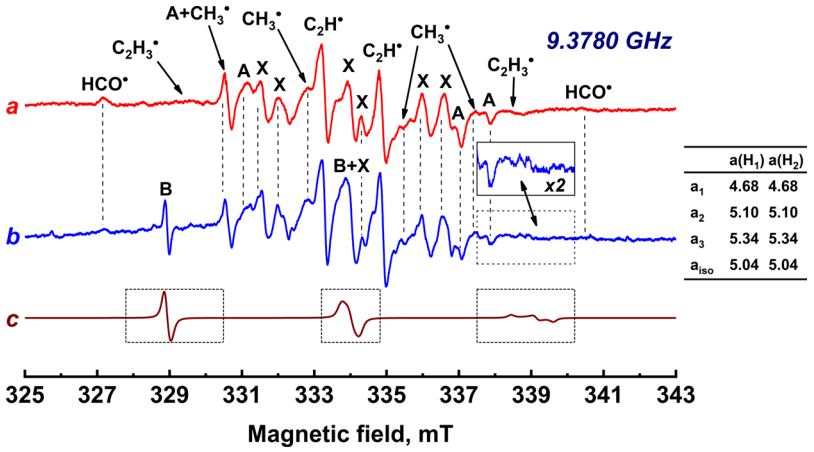

Figure 7. EPR spectra (recorded at 5 K) of the $^{12}C_2H_2/CO/CFCl_3/Ar$ 1:3:1:1000 sample illustrating the effect of 15 min radiolysis (*a*), subsequent photolysis of the irradiated sample with λ_D = 465 nm light for 75 min (*b*), and simulation (*c*) of the feature **B** (see text for details). HFC constants (mT) extracted from the simulation of the **B** feature are provided in the right panel. Both spectra are normalized to the peak intensity of the $C_2H^•$ signals. Simulation areas are marked with dashed frames. Experimental microwave frequency is provided in the top right corner.

above-mentioned magnetic field regions of 330.0−331.4 and 336.7−338.1 mT. In order to make a choice between different structures, we should address the results of calculations.

Generally speaking, all the $H_2{}^{12}C_3O^{+•}$ species have two protons, and they should yield a doublet of doublet spectral pattern, which degenerates to triplet in case both protons are equivalent (structures **I** and **II**). These two latter structures can be ruled out because we do not observe any clear sign of a central feature corresponding to the M_I = 0 characteristic of a triplet signal. The total spread of the signal resulting from two inequivalent protons is determined by the sum of the absolute values of HFC constants. Apparently, the total spread expected for structures **VI** (primary complex) and **IVb** (Z-HCCHCO$^{+•}$ isomer) is too small to account for the observed outermost features **A** separated by ca. 7 mT. On the other hand, the value of the HFC constant with one of the protons for isomer **III** seems to be too large (additionally we may note that, according to the energy diagram presented in Figure 1, it is a high-energy isomer and its formation looks highly unlikely). Thus, the most reasonable candidate is structure **IVa** (*E*-HCCHCO$^{+•}$ isomer). To confirm this suggestion and to extract the HFC parameters from the experiment, we have carried out a series of anisotropic powder simulations.

We may note that the simulation is not straightforward in this case because of the presence of the signals from many species, some of which cannot be unambiguously identified (see above). In order to simplify the procedure and make it more reliable, first, we have restricted consideration to the informative magnetic field regions ignoring the central part of the spectrum between 332 and 336 mT. The contributions of the signals from vinyl and methyl radicals in the selected regions were neglected because of their very low intensity in comparison with those of **A** and **X**. The signal of the acetylene-related species **X** in the informative magnetic field regions was taken from the EPR spectra of the $C_2H_2/CFCl_3/Ar$ irradiated sample (Figure 6, *d*). The result of fitting the experimental spectrum by the sum of **A** (model assuming the presence of two inequivalent protons with variable *g* and HFC tensors, and line width) and **X** is shown in Figure 6, *b*, and the neat simulation of **A** corresponding to this fit is shown in Figure 6, *c*. The best-fit HFC parameters for **A** are listed in Figure 6, and the complete set of parameters for **A** and **X** corresponding to the best-fit simulation is given in Table S8 of the SI. Comparing these results with the calculated values for **IVa** (Table 3), we can see that the agreement is satisfactory within 20−25%. We have to stress that the calculated values for all other structures are inconsistent with fitted parameters extracted from the experiment. Further consideration of these results will be given in the Concluding Discussion.

Additional proof of the identity of the species assigned to the radical cation **IVa** from the EPR data and a cationic species responsible for absorption **A** in the IR spectra was obtained in photochemical studies. As shown in Figure 7, photolysis of the irradiated $^{12}C_2H_2/CO/CFCl_3/Ar$ 1:3:1:1000 sample with a λ_D = 465 nm light results in noticeable transformations in the observed EPR spectrum (see Figure 7). It is worth noting that we used the signal of $C_2H^•$ radicals, which are not affected by photolysis (according to the FTIR matrix isolation data), as an internal reference for semiquantitative estimations. The formyl radical disappears under photolysis, which agrees with its well-known photosensitivity in the visible region (see, for example, ref 93). Simultaneously, the intensity of features **A** decreases, demonstrating some kind of photoinduced transformation. The most interesting result is the appearance of two new photoinduced features marked as **B**, which may correspond to the photoinduced absorption **B** observed in the IR spectrum (see the previous subsection). The first line (well-defined and relatively narrow) appears in the low-field region at 328.4 mT, while the second broader feature rises in the centrum of the spectrum (at 333.4 mT), overlapping with the signal present before photolysis and tentatively belonging to an acetylene-related species **X**. The distance between the features marked as **B** is ca. 5.0 mT. We failed to find any feature with comparable intensity in the 338.4 mT region. It should be pointed out that the features marked as **B** definitely result from a photosensitive species originating from the irradiated $C_2H_2\cdots CO$ complex and not from a product of $CFCl_3$ radiolysis; because they are not observed in the photolyzed $^{13}C_2H_2/CO/CFCl_3/Ar$ samples (see Figure S5 of the SI). The interpretation of signal **B** is somewhat complicated because, at first glance, it could belong to a paramagnetic species with a strong positive shift of the *g*-value in comparison with the g_e region, which looks very unusual. However, taking into account anisotropic line broadening, we may suggest that the spectrum of **B** actually

https://doi.org/10.1021/jacs.2c00295
J. Am. Chem. Soc. 2022, 144, 8115−8128

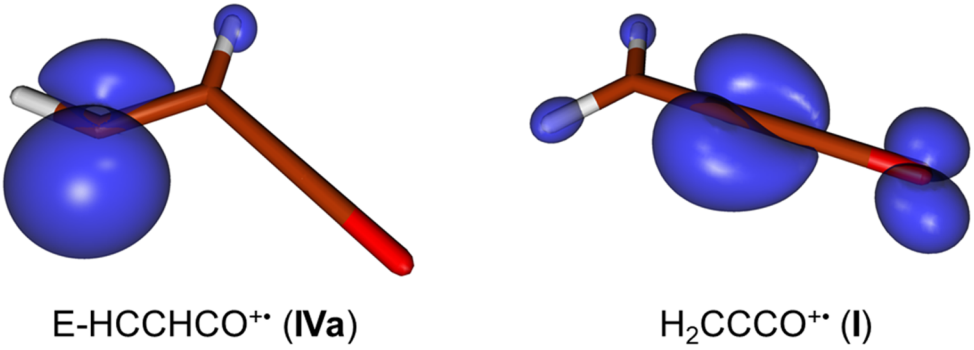

Figure 8. Spin density (within a 0.01 au value) of the *E*-HCCHCO$^{+\bullet}$ (**IVa**) and $H_2CCCO^{+\bullet}$ (**I**) isomers calculated at the UCCSD(T)/L3a_3//UCCSD(T)/L3a_3 level of theory.

contains a low-intensity and broad high-field component, which is hardly seen in a powder-type spectral pattern. If this is the case, the photoinduced signal represents a triplet from two equivalent protons with a total spread of ca. 10 mT, where the high-field component is hidden due to severe line broadening. Such a situation corresponds to a species with two strongly interacting protons ($a \approx 5$ mT), which is characteristic of structure **I** (see Table 3). The powder simulation with least-squares fitting yields the pattern shown in Figure 7. The principal components of the HFC tensor extracted from fitting are given in Figure 7 (the full set of best-fit parameters is provided in Table S8 of the SI). These values are indeed rather close to those calculated for **I** (see Table 3). Thus, on the basis of EPR results, we can reasonably identify the photoinduced feature **B** as the $H_2CCCO^{+\bullet}$ radical cation. The corresponding orbital spin density distribution is illustrated in Figure 8.

CONCLUDING DISCUSSION

The experimental results obtained in this work strongly suggest that the key intermediate resulting from ionization of the $C_2H_2\cdots CO$ complex in matrices should be identified as the *E*-HCCHCO$^{+\bullet}$ isomer of the $H_2C_3O^{+\bullet}$ radical cation (structure **IVa**). The spectroscopic signatures of this species are intense absorption related to the C═O stretching vibrations in the FTIR spectrum and characteristic proton HFC revealed by EPR. We may note that the spectroscopic arguments given above are supported by thermodynamic and kinetic considerations. Indeed, according to the energy diagram given in Figure 1, the *E*-HCCHCO$^{+\bullet}$ radical cation represents a rather deep local minimum protected from further rearrangements by relatively high barriers. Furthermore, its hypothetic fragmentation to $C_3O^{+\bullet}$ and H_2 or HC_3O^+ and H$^\bullet$ is noticeably endothermic (see the Computational Results section). From the kinetic point of view, it is worth noting that accumulation of the species in focus upon irradiation of C_2H_2/CO/Ar samples at relatively low absorbed doses is accompanied by the formation of the C_2H^- anion (band at 1768.6 and 1716.3 cm^{-1} for $^{12}C_2H^-$ and $^{13}C_2H^-$, respectively),[94,95] which probably originates from the electron scavenging by the $C_2H^\bullet$ radical, the major product of acetylene radiolysis in matrices. The formation of noticeable amounts of the C_2H^- anion in the C_2H_2/CO/Ar system definitely indicates charge separation in this case, where the $C_2H_2\cdots CO$ complex acts as a hole trap. When the concentration of the $H_2C_3O^{+\bullet}$ radical cation increases, it starts competing with the $C_2H^\bullet$ radical for electrons, which naturally explains the appearance of the maximum in the $H_2C_3O^{+\bullet}$ amount at the complex conversion degree above 10% (Figure 3).

To the best of our knowledge, the *E*-HCCHCO$^{+\bullet}$ radical cation was not characterized previously by any spectroscopic technique, so it is worth briefly commenting on its structural features. First, we may note that this species demonstrates the shortest C═O bond length of all the isomers of the $H_2C_3O^{+\bullet}$ radical cation (including the primary ionized complex), which correlates with the highest value of the corresponding computed stretching frequency. Second, considering the geometric structure, one could notice its certain resemblance to that of the vinyl radical,[87] where one of the H$^\bullet$ atoms of the CH_2 group is replaced by a nine-electron $CO^{+\bullet}$ fragment. Indeed, the largest isotropic proton HFC in the vinyl radical corresponds to the H atom taking the position analogous to H_1 nucleus in structure **IVa**. This value is known to be 6.59 mT,[91] which is quite comparable with the value of 6.35 mT for H_1 nucleus in the *E*-HCCHCO$^{+\bullet}$ radical cation extracted from the EPR data obtained in this work. The CH terminal proton (H_2 nucleus in structure **IVa**) exhibits a much smaller coupling constant for both the vinyl radical and *E*-HCCHCO$^{+\bullet}$ radical cation (1.38 and 0.43 mT, respectively). These data generally identify both species as σ-type radicals (as illustrated by the spin density distribution presented in Figure 8 for the *E*-HCCHCO$^{+\bullet}$ radical cation) and may imply some similarity in their reactivity.

The whole evolution of the $C_2H_2\cdots CO$ complex after ionization represents an interesting example of a kinetically controlled low-temperature synthetic chemistry with a "frozen" metastable state. Apparently, the ionization of the complex immediately leads to its barrierless transformation to a Z-HCCHCO$^{+\bullet}$ radical cation (structure **IVb**). However, this intermediate is not trapped under the conditions of the matrix isolation experiment. Most probably, the excess energy of the ionized system is sufficient to overcome a quite low energy barrier (1.71 kcal mol^{-1}, **TS2** in Figure 1); also, the involvement of tunnelling in a low-barrier isomerization **IVb** → **IVa** cannot be excluded. Thus, the system proceeds to the "frozen" state **IVa**, which is protected from further transformations by relatively high barriers (more than 12 kcal mol^{-1}), and it is this intermediate that is trapped in the matrix and observed experimentally. We have to stress that further transformations of the $H_2C_3O^{+\bullet}$ radical cations theoretically predicted on the ground-state PES (right part of Figure 1) do not occur under radiolysis in the experimental conditions used in this work. We may suggest that the neutral molecular and radical products observed in the irradiated C_2H_2/CO/Ar

https://doi.org/10.1021/jacs.2c00295
J. Am. Chem. Soc. 2022, 144, 8115−8128

system[58] most probably originate from neutral excited states formed by recombination of the *E*-$HCCHCO^{+\bullet}$ radical cations with electrons, as supported by kinetic consideration and the effect of electron scavenger.

The photoisomerization of *E*-$HCCHCO^{+\bullet}$ to the $H_2CCCO^{+\bullet}$ radical cation (**IVa** → **I**) experimentally observed in this work is a rather interesting and unusual reaction (still not reported in either the gas or condensed phase). If we consider the ground state doublet PES, the calculated energy barrier is ca. 1.73 eV (Figure 1), so the energy of blue light used in this work (ca. 2.7 eV) is definitely sufficient to induce such transformations. However, at this stage, we would refrain from the detailed description of the pathway responsible for this transformation since the computation of the excited state doublet PES is a very demanding task, which may present a challenge for further theoretical investigations.

It should be noted that both **IVa** and **I** isomers of $H_2C_3O^{+\bullet}$ are expected to be thermodynamically stable in an Ar matrix, because the computations show their deprotonation (via formal reaction $H_2C_3O^{+\bullet} + Ar_2 \rightarrow HC_3O^{\bullet} + Ar_2H^+$) to be unfavorable by more than 80 kcal mol^{-1} (see the results presented in Table S3 of the SI). This is in line with experimental observations, which reveal complete stability of the signals ascribed to both radical cations in the time scale of, at least, several hours.

Finally, we have to comment on the direct and indirect implications of the obtained results for different areas of chemistry. Focusing on the $C_2H_2\cdots CO$ complex as one of the most important building blocks in cold synthetic astrochemistry,[58] we may stress the potential importance of cationic pathways in its transformations. While the earlier discussions of the evolution of this system were mainly based on the consideration of neutral reactions,[55−57] here we have explicitly shown that the ionic transformations and formation of related intermediates may be crucially significant in model matrices, and this may also be the case for astrophysical ices. In a wider chemical context, we believe that this study demonstrates a prominent example of confined synthetic chemistry starting from simple isolated complexes, which occurs at extremely low temperatures. In particular, such an approach can be used for the preparation and stabilization of basically important small radical cations corresponding to the ionization of unusual or unstable molecules. The possibility of their detailed characterization by vibrational and EPR spectroscopy and comparison with advanced computational investigations could provide unique information on their identity and electronic and molecular structure, which is often unavailable in the common gas-phase ionization studies. Furthermore, an interesting opportunity is concerned with selective matrix-controlled chemistry that can be revealed in such experiments. In principle, the matrix can determine the selection of the close in energy isomers of the radical cations (such as the *E*- or Z-isomers of $HCCHCO^{+\bullet}$ discussed in this work); such examples for hydrocarbon radical cations in halocarbon and noble gas matrices are indeed known (see, for example, refs 96 and 97). Potentially this could be the basis for stereoselective chemistry at extremely low temperatures characteristic of the conditions of cold space media.

SUMMARY

In this work, we have analyzed the low-temperature transformations occurring in the ionized 1:1 $C_2H_2\cdots CO$ complex from theoretical and experimental points of view. The calculations revealed six isomers of the common $H_2C_3O^{+\bullet}$ formula: $H_2CCCO^{+\bullet}$ (**I**), c-$H_2C_3O^{+\bullet}$ (**II**), $HCCCHO^{+\bullet}$ (**III**), *E*-$HCCHCO^{+\bullet}$ (**IVa**), *Z*-$HCCHCO^{+\bullet}$ (**IVb**), and ionized $(C_2H_2\cdots CO)^{+\bullet}$ complex (**VI**). The relative energy of these isomers increases in a row, **I** < **IVa** ∼ **IVb** < **II** < **III** < **VI**, in general agreement with previous calculations.[42,43] It was found that the primary ionized complex (**VI**) could undergo virtually barrierless rearrangement to the **IVb** isomer, and conversion of the latter species to a more stable **IVa** isomer is characterized by a relatively low barrier (1.71 kcal mol^{-1}). In contrast, the **IVa** isomer is protected from further transformations to the **III**, **II**, and **I** isomers by rather high energy barriers (48.77, 12.48, and 39.81 kcal mol^{-1}, respectively).

The argon matrix isolation experiments revealed that the $H_2C_3O^{+\bullet}$ radical cation is formed as a result of the radiation-induced transformations of the matrix-isolated $C_2H_2\cdots CO$ complex. Comparison of the experimentally obtained FTIR and EPR parameters with calculated values demonstrated that the observed species should be described as *E*-$HCCHCO^{+\bullet}$ (**IVa**). Photolysis of the **IVa** radical cation results in its rearrangement into the most thermodynamically stable $H_2CCCO^{+\bullet}$ structure (**I**), which was also characterized by a combination of the FTIR and EPR spectroscopy. The obtained results suggest that kinetic control plays a dominant role in the observed chemical selectivity. It is worth noting that the H_2C_3O isomers (propynal, cyclopropenone, and propadienone) represent a prominent example of minimum energy principle violation, which states that the most thermodynamically stable isomer should be more abundant in the ISM. At the same time, propadienone, which is the most thermodynamically stable isomer, is still not found in the extraterrestrial media in contrast to propynal and cyclopropenone. Thus, kinetics rather than thermodynamics should be crucial for the production of the H_2C_3O species in the ISM.[98−101]

Taking into account the results obtained in our previous work[58] we may suggest that the *E*-$HCCHCO^{+\bullet}$ radical cation should be the key intermediate in the radiation-induced transformations occurring in the C_2H_2−CO system, which may noticeably contribute to the radiolytic formation of H_2C_3O isomers (namely, propynal and cyclopropenone) and presumably more complex species in the mixed C_2H_2−CO ices at 10 K.[55−57] We believe that the strategy of preparation and characterization of small organic radical cations used in this study may be applied to a rather wide class of systems representing great interest for astrochemistry as well as for physical organic chemistry.

ASSOCIATED CONTENT

Supporting Information

The Supporting Information is available free of charge at https://pubs.acs.org/doi/10.1021/jacs.2c00295.

Results of the quantum-chemical calculations (optimized molecular geometries and energies, harmonic frequencies, and IR intensities of the investigated species); optimized EPR parameters of the radical cations obtained by the least-squares fitting procedure of the experimental data; results of the $^{13}C_2H_2$/CO/$CFCl_3$/Ar EPR studies (PDF)

https://doi.org/10.1021/jacs.2c00295
J. Am. Chem. Soc. 2022, 144, 8115−8128

AUTHOR INFORMATION

Corresponding Author

Vladimir I. Feldman − *Department of Chemistry, Lomonosov Moscow State University, 119991 Moscow, Russia;* orcid.org/0000-0002-5407-8685; Email: feldman@rad.chem.msu.ru

Authors

Pavel V. Zasimov − *Department of Chemistry, Lomonosov Moscow State University, 119991 Moscow, Russia;* orcid.org/0000-0003-0337-5927

Daniil A. Tyurin − *Department of Chemistry, Lomonosov Moscow State University, 119991 Moscow, Russia*

Sergey V. Ryazantsev − *Center for Energy Science and Technology, Skolkovo Institute of Science and Technology, 121205 Moscow, Russia; Department of Chemistry, Lomonosov Moscow State University, 119991 Moscow, Russia;* orcid.org/0000-0001-8662-580X

Complete contact information is available at: https://pubs.acs.org/10.1021/jacs.2c00295

Author Contributions

The manuscript was written through contributions of all authors. All authors have given approval to the final version of the manuscript.

Funding

This work was supported by the Russian Foundation for Basic Research (grant no. 19-03-00579-a).

Notes

The authors declare no competing financial interest.

ACKNOWLEDGMENTS

The Joint Supercomputer Center of the Russian Academy of Sciences (JSCC RAS) is acknowledged for granting computation resources. The continuous experimental assistance from I. V. Tyulpina is gratefully acknowledged. The authors thank Dimitri N. Laikov for designing and building a new electronic circuit for the EPR spectrometer's magnetic field control and stabilization, and Natalia V. Feldman for developing new EPR spectrometer control software with a graphical user interface.

REFERENCES

(1) Schmittel, M.; Burghart, A. Understanding reactivity patterns of radical cations. *Angew. Chem., Int. Ed.* **1997**, *36* (23), 2550−2589.

(2) Fokin, A. A.; Schreiner, P. R. Selective alkane transformations via radicals and radical cations: Insights into the activation step from experiment and theory. *Chem. Rev.* **2002**, *102* (5), 1551−1594.

(3) Snow, T. P.; Bierbaum, V. M. Ion chemistry in the interstellar medium. *Annu. Rev. Anal. Chem.* **2008**, *1*, 229−259.

(4) Todres, Z. V. *Ion-Radical Organic Chemistry: Principles and Applications*, 2nd ed.; CRC Press, Taylor & Fransis Group: Boca Raton, FL, USA, 2008; p 496.

(5) Forbes, M. D., Ed. *Carbon-Centered Free Radicals and Radical Cations: Structure, Reactivity, and Dynamics*, Vol. 2; John Wiley & Sons, Inc.: Hoboken, NJ, 2010; p 370.

(6) Lin, S.; Ischay, M. A.; Fry, C. G.; Yoon, T. P. Radical cation Diels−Alder cycloadditions by visible light photocatalysis. *J. Am. Chem. Soc.* **2011**, *133* (48), 19350−19353.

(7) Campbell, J. M.; Xu, H. C.; Moeller, K. D. Investigating the Reactivity of Radical Cations: Experimental and Computational Insights into the Reactions of Radical Cations with Alcohol and p-Toluene Sulfonamide Nucleophiles. *J. Am. Chem. Soc.* **2012**, *134* (44), 18338−18344.

(8) Ischay, M. A.; Yoon, T. P. Accessing the synthetic chemistry of radical ions. *Eur. J. Org. Chem.* **2012**, *18*, 3359−3372.

(9) Larsson, M.; Geppert, W. D.; Nyman, G. Ion chemistry in space. *Rep. Prog. Phys.* **2012**, *75* (6), 066901.

(10) Wu, S.; Žurauskas, J.; Domański, M.; Hitzfeld, P. S.; Butera, V.; Scott, D. J.; Rehbein, J.; Kumar, A.; Thyrhaug, E.; Hauer, J.; Barham, J. P. Hole-mediated photoredox catalysis: tris(p-substituted)-biarylaminium radical cations as tunable, precomplexing and potent photooxidants. *Org. Chem. Front.* **2021**, *8* (6), 1132−1142.

(11) Collins, J. R.; Gallup, G. A. Energy surfaces in the cyclopropane radical ion and the photoelectron spectrum of cyclopropane. *J. Am. Chem. Soc.* **1982**, *104* (6), 1530−1533.

(12) Bouma, W. J.; MacLeod, J. K.; Radom, L. Experimental evidence for the existence of a stable isomer of $CH_3OH^{+\bullet}$: the methylenoxonium radical cation, $CH_2OH_2^{+\bullet}$. *J. Am. Chem. Soc.* **1982**, *104* (10), 2930−2931.

(13) van Baar, B.; Weiske, T.; Terlouw, J. K.; Schwarz, H. Hydroxyacetylene: Generation and characterization of the neutral molecule, radical cation and dication in the gas phase. *Angew. Chem., Int. Ed.* **1986**, *25* (3), 282−284.

(14) Hammerum, S. Distonic radical cations in gaseous and condensed phase. *Mass Spectrom. Rev.* **1988**, *7* (2), 123−202.

(15) Blush, J. A.; Clauberg, H.; Kohn, D. W.; Minsek, D. W.; Zhang, X.; Chen, P. Photoionization mass and photoelectron spectroscopy of radicals, carbenes, and biradicals. *Acc. Chem. Res.* **1992**, *25* (9), 385−392.

(16) Lund, A.; Shiotani, M., Eds. *Radical Ionic Systems: Properties in Condensed Phases*, Vol. 6; Springer Science & Business Media, 2012; p 496.

(17) Kondoh, T.; Yang, J.; Norizawa, K.; Kan, K.; Yoshida, Y. Femtosecond pulse radiolysis study on geminate ion recombination in n-dodecane. *Radiat. Phys. Chem.* **2011**, *80* (2), 286−290.

(18) Kondoh, T.; Yang, J.; Norizawa, K.; Kan, K.; Kozawa, T.; Ogata, A.; Tagawa, S.; Yoshida, Y. Femtosecond pulse radiolysis study of geminate ion recombination in biphenyl−dodecane solution. *Radiat. Phys. Chem.* **2013**, *84*, 30−34.

(19) Bally, T. In *Reactive Intermediate Chemistry*; Moss, R. A.; Platz, M. S.; Jones, M., Jr., Eds.; John Wiley & Sons, Inc.: NJ, 2003; pp 795−845.

(20) Knight, L. B., Jr. ESR investigations of molecular cation radicals in neon matrices at 4 K: generation, trapping, and ion-neutral reactions. *Acc. Chem. Res.* **1986**, *19* (10), 313−321.

(21) Jacox, M. E.; Thompson, W. E. The production and spectroscopy of molecular ions isolated in solid neon. *Res. Chem. Intermed.* **1989**, *12*, 33−56.

(22) Bondybey, V. E.; Smith, A. M.; Agreither, J. New developments in matrix isolation spectroscopy. *Chem. Rev.* **1996**, *96*, 2113−2134.

(23) Feldman, V. I. In *Application of EPR in Radiation Research*; Lund, A.; Shiotani, M., Eds.; Springer: Cham, 2014; pp 151−188.

(24) Goldschleger, I. U.; Akimov, A. V.; Misochko, E. Y.; Wight, C. A. EPR and infrared spectra of the HFC = $N^{\bullet}$ free radical stabilised in solid argon. *Mend. Comm.* **2001**, *11* (2), 64−66.

(25) Sato, T.; Narazaki, A.; Kawaguchi, Y.; Niino, H.; Bucher, G.; Grote, D.; Wolff, J.; Wenk, H. H.; Sander, W. Generation and photoreactions of 2,4,6-trinitreno-1,3,5-triazine, a septet trinitrene. *J. Am. Chem. Soc.* **2004**, *126* (25), 7846−7852.

(26) Neuhaus, P.; Sander, W. Isolation and Characterization of the Triradical 1,3,5-Trimethylenebenzene. *Angew. Chem., Int. Ed.* **2010**, *122* (40), 7435−7438.

(27) Costa, P.; Lohmiller, T.; Trosien, I.; Savitsky, A.; Lubitz, W.; Fernandez-Oliva, M.; Sanchez-Garcia, E.; Sander, W. Light and Temperature Control of the Spin State of Bis(p-methoxyphenyl)-carbene: A Magnetically Bistable Carbene. *J. Am. Chem. Soc.* **2016**, *138* (5), 1622−1629.

(28) Gutiérrez-Quintanilla, A.; Layssac, Y.; Butscher, T.; Henkel, S.; Tsegaw, Y. A.; Grote, D.; Sander, W.; Borget, F.; Chiavassa, T.; Duvernay, F. iCOM formation from radical chemistry: a mechanistic study from cryogenic matrix coupled with IR and EPR spectroscopies. *Mon. Not. R. Astron. Soc.* **2021**, *506* (3), 3734−3750.

(29) Kelsall, B. J.; Andrews, L. Absorption spectra and photochemical rearrangements of toluene, cycloheptatriene, and norbornadiene cations to methylenecyclohexadiene cation in solid argon. *J. Am. Chem. Soc.* **1983**, *105* (6), 1413−1419.
(30) Bally, T.; Nitsche, S.; Roth, K.; Haselbach, E. Excited states of polyene radical cations: limitations of Koopmans' theorem. *J. Am. Chem. Soc.* **1984**, *106* (14), 3927−3933.
(31) Mondal, R.; Tönshoff, C.; Khon, D.; Neckers, D. C.; Bettinger, H. F. Synthesis, stability, and photochemistry of pentacene, hexacene, and heptacene: A matrix isolation study. *J. Am. Chem. Soc.* **2009**, *131* (40), 14281−14289.
(32) Muller, B.; Bally, T.; Pappas, R.; Williams, F. Spectroscopic and Computational Studies on the Rearrangement of Ionized [1.1.1]-Propellane and Some of its Valence Isomers: The Key Role of Vibronic Coupling. *J. Am. Chem. Soc.* **2010**, *132* (41), 14649−14660.
(33) Ryazantsev, S. V.; Feldman, V. I. Matrix-Isolation Studies on the Radiation-Induced Chemistry in H_2O/CO_2 Systems: Reactions of Oxygen Atoms and Formation of HOCO Radical. *J. Phys. Chem. A* **2015**, *119* (11), 2578−2586.
(34) Ryazantsev, S. V.; Duarte, L.; Feldman, V. I.; Khriachtchev, L. VUV photochemistry of the $H_2O\cdots CO$ complex in noble-gas matrices: formation of the $OH\cdots CO$ complex and the HOCO radical. *Phys. Chem. Chem. Phys.* **2017**, *19*, 356−365.
(35) Changyun, C.; Lu, B.; Zhao, X.; Quian, W.; Liu, J.; Trabelsi, T.; Francisco, J. S.; Qin, J.; Li, J.; Wang, L.; Zen, X. Capture of the Sulfur Monoxide−Hydroxyl Radical Complex. *J. Am. Chem. Soc.* **2020**, *142*, 2175−2179.
(36) Zasimov, P. V.; Ryazantsev, S. V.; Tyurin, D. A.; Feldman, V. I. Radiation-induced chemistry in the $C_2H_2-H_2O$ system at cryogenic temperatures: a matrix isolation study. *Mon. Not. R. Astron. Soc.* **2020**, *491* (4), 5140−5150.
(37) Ryazantsev, S. V.; Zasimov, P. V.; Feldman, V. I. Radiation-induced synthesis of formic acid in the H_2O-CO system: A matrix isolation study. *Chem. Phys. Lett.* **2020**, *753*, 137540.
(38) Lukianova, M. A.; Volosatova, A. D.; Drabkin, V. D.; Sosulin, I. S.; Kameneva, S. V.; Feldman, V. I. Radiation-induced transformations of $HCN\cdots C_2H_2$, $HCN\cdots C_2H_4$ and $HCN\cdots C_2H_6$ complexes in noble gas matrices: Synthesis of C_3H_xN molecules in cryogenic media. *Radiat. Phys. Chem.* **2020**, 109232.
(39) Feldman, V. I.; Ryazantsev, S. V.; Saenko, E. V.; Kameneva, S. V.; Shiryaeva, E. S. Matrix isolation model studies on the radiation-induced transformations of small molecules of astrochemical and atmospheric interest. *Radiat. Phys. Chem.* **2016**, *124*, 7−13.
(40) Arumainayagam, C. R.; Garrod, R. T.; Boyer, M. C.; Hay, A. K.; Bao, S. T.; Campbell, J. S.; Wang, J.; Nowak, C. M.; Arumainayagam, M. R.; Hodge, P. J. Extraterrestrial prebiotic molecules: photochemistry vs. radiation chemistry of interstellar ices. *Chem. Soc. Rev.* **2019**, *48*, 2293−2314.
(41) Feldman, V. I.; Ryazantsev, S. V.; Kameneva, S. V. Matrix isolation in laboratory astrochemistry: state-of-the-art, implications and perspective. *Russ. Chem. Rev.* **2021**, *90* (9), 1142−1165.
(42) Bouchoux, G.; Hoppilliard, Y.; Flament, J. P.; Terlouw, J. K.; Van der Valk, F. Experimental and theoretical study of $[C_3H_2O]^{+\bullet}$ cations. Evidence for the existence of stable $[CH=CH-CO]^{+\bullet}$ ions in the gas phase. *J. Phys. Chem.* **1986**, *90*, 1582−1585.
(43) Holmes, J. L.; Jobst, K. J.; Terlouw, J. K. Small (Poly)-Unsaturated Oxygen Containing Ions and Molecules: A Brief Assessment of Their Thermochemistry Based on Computational Chemistry. *Eur. J. Mass. Spectrom.* **2009**, *15* (2), 261−273.
(44) Terlow, J. K.; Holmes, J. H.; Lossing, F. P. Ionized ethylidene ketene and its homologue methylene ketene. *Can. J. Chem.* **1983**, *61* (8), 1722−1724.
(45) Maquestiau, A.; Pauwels, P.; Flammang, R.; Lorencak, P.; Wentrup, C. Unsaturated ketenes: A study of their formation and rearrangement by tandem mass spectrometry and low-temperature infrared spectroscopy. *Organic Mass Spectrometry* **1986**, *21* (5), 259−265.
(46) Harshbarger, W. R.; Kuebler, N. A.; Robin, M. B. Electronic structure and spectra of small rings. V Photoelectron and electron impact spectra of cyclopropenone. *J. Chem. Phys.* **1974**, *60* (2), 345−350.
(47) von Niessen, W.; Bieri, G.; Åsbrink, L. 30.4-nm He (II) photoelectron spectra of organic molecules: Part III. Oxo-compounds (C, H, O). *J. Electron Spectrosc. Relat. Phenom.* **1980**, *21* (2), 175−191.
(48) Opitz, J. Photoionization of propynal in the gas phase. *Int. J. Mass. Spectrom.* **1991**, *107* (3), 503−513.
(49) Derbali, I.; Hrodmarsson, H. R.; Gouid, Z.; Schwell, M.; Gazeau, M. C.; Guillemin, J. C.; Hochlaf, M.; Alikhani, M. E.; Zins, E. L. Photoionization and dissociative photoionization of propynal in the gas phase: theory and experiment. *Phys. Chem. Chem. Phys.* **2019**, *21* (26), 14053−14062.
(50) Herbst, E.; Smith, D.; Adams, N. G. Ion−molecule synthesis of C_3O. *Astron. Astrophys.* **1984**, *138*, L13−L14.
(51) Adams, N. G.; Smith, D.; Giles, K.; Herbst, E. The production of C_nO, HC_nO, and H_2C_nO molecules in dense interstellar clouds. *Astron. Astrophys.* **1989**, *220*, 269−271.
(52) Petrie, S.; Bettens, R. P.; Freeman, C. G.; McEwan, M. J. The ion chemistry of $H_nC_3O^+$, $C_3O_2^+$ and C_3O^+ in dense interstellar clouds: an experimental study. *Mon. Not. R. Astron. Soc.* **1993**, *264*, 862−864.
(53) Petrie, S.; Bettens, R. P.; Freeman, C. G.; McEwan, M. J. Ion−molecule chemistry of $H_nC_3O^+$, $C_3O_2^+$, and C_3O^+. *J. Phys. Chem.* **1993**, *97* (51), 13673−13676.
(54) Urso, R. G.; Palumbo, M. E.; Ceccarelli, C.; Balucani, N.; Bottinelli, S.; Codella, C.; Fontani, F.; Leto, P.; Trigilio, C.; Vastel, C.; Bachiller, R.; Baratta, G. A.; Buemi, C. S.; Caux, E.; Jaber Al-Edhari, A.; Lefloch, B.; López-Sepulcre, A.; Umana, G.; Testi, L. C_2O and C_3O in low-mass star-forming regions. *Astron. Astrophys.* **2019**, *628*, A72.
(55) Zhou, L.; Kaiser, R. I.; Gao, L. G.; Chang, A. H.; Liang, M. C.; Yung, Y. L. Pathways to oxygen-bearing molecules in the interstellar medium and in planetary atmospheres: cyclopropenone (c-C_3H_2O) and propynal (HCCCHO). *Astrophys. J.* **2008**, *686*, 1493−1502.
(56) Abplanalp, M. J.; Kaiser, R. I. On the formation of complex organic molecules in the interstellar medium: untangling the chemical complexity of carbon monoxide−hydrocarbon containing ice analogues exposed to ionizing radiation via a combined infrared and reflectron time-of-flight analysis. *Phys. Chem. Chem. Phys.* **2019**, *21*, 16949.
(57) Kleimeier, N. F.; Abplanalp, M. J.; Johnson, R. N.; Gozem, S.; Wandishin, J.; Shingledecker, C. N.; Kaiser, R. I. Cyclopropenone (c-C_3H_2O) as a Tracer of the Nonequilibrium Chemistry Mediated by Galactic Cosmic Rays in Interstellar Ices. *Astrophys. J.* **2021**, *911* (1), 24.
(58) Zasimov, P. V.; Ryazantsev, S. V.; Tyurin, D. A.; Feldman, V. I. $C_2H_2\cdots CO$ complex and its radiation-induced transformations: a building block for cold synthetic astrochemistry. *Mon. Not. R. Astron. Soc.* **2021**, *506* (3), 3499−3510.
(59) Laikov, D. N.; Ustynyuk, Y. A. PRIRODA-04: a quantum-chemical program suite. New possibilities in the study of molecular systems with the application of parallel computing. *Russ. Chem. Bull.* **2005**, *54*, 820−826.
(60) Raghavachari, K.; Trucks, G. W.; Pople, J. A.; Head-Gordon, M. A fifth-order perturbation comparison of electron correlation theories. *Chem. Phys. Lett.* **1989**, *157*, 479−483.
(61) Laikov, D. N. Atomic basis functions for molecular electronic structure calculations. *Theor. Chem. Acc.* **2019**, *138*, 40.
(62) Dunning, T. H. Gaussian basis sets for use in correlated molecular calculations. I. The atoms boron through neon and hydrogen. *J. Chem. Phys.* **1989**, *90*, 1007−1023.
(63) Kendall, R. A.; Dunning, T. H.; Harrison, R. J. Electron affinities of the first-row atoms revisited. Systematic basis sets and wave functions. *J. Chem. Phys.* **1992**, *96*, 6796−6806.
(64) Woon, D. E.; Dunning, T. H. Gaussian basis sets for use in correlated molecular calculations. III. The atoms aluminum through argon. *J. Chem. Phys.* **1993**, *98*, 1358−1371.

https://doi.org/10.1021/jacs.2c00295
J. Am. Chem. Soc. 2022, 144, 8115−8128

(65) Woon, D. E.; Dunning, T. H. Gaussian basis sets for use in correlated molecular calculations. IV. Calculation of static electrical response properties. *J. Chem. Phys.* **1994**, *100*, 2975−2988.
(66) Wilson, A. K.; Woon, D. E.; Peterson, K. A.; Dunning, T. H. Gaussian basis sets for use in correlated molecular calculations. IX. The atoms gallium through krypton. *J. Chem. Phys.* **1999**, *110*, 7667−7676.
(67) Sosulin, I. S.; Tyurin, D. A.; Feldman, V. I. A hydrogen-bonded CH_2F_2···CO complex: ab initio and matrix isolation study. *J. Mol. Struct.* **2020**, *1221*, 128784.
(68) Sosulin, I. S.; Tyurin, D. A.; Feldman, V. I. A hydrogen-bonded CHF···HF complex: IR spectra and unusual photochemistry. *J. Chem. Phys.* **2021**, *154*, 104310.
(69) Sosulin, I. S.; Feldman, V. I. Spectroscopy and radiation-induced chemistry of an atmospherically relevant CH_2F_2···H_2O complex: Evidence for the formation of CF_2···H_2O complex as revealed by FTIR matrix isolation and ab initio study. *Chemosphere* **2022**, *291*, 132967.
(70) Schaftenaar, G.; Noordik, J. H. Molden: a pre-and post-processing program for molecular and electronic structures. *J. Comput. Aided Mol. Des.* **2000**, *14*, 123−134.
(71) Schaftenaar, G.; Vlieg, E.; Vriend, G. Molden 2.0: quantum chemistry meets proteins. *J. Comput. Aided Mol. Des.* **2017**, *31*, 789−800.
(72) Bartlett, R. J.; Park, Y. C.; Bauman, N. P.; Melnichuk, A.; Ranasinghe, D.; Ravi, M.; Perera, A. Index of multi-determinantal and multi-reference character in coupled-cluster theory. *J. Chem. Phys.* **2020**, *153*, 234103.
(73) Cioslowski, J. A new population analysis based on atomic polar tensors. *J. Am. Chem. Soc.* **1989**, *111*, 8333−8336.
(74) Saenko, E. V.; Feldman, V. I. Radiation-induced transformations of methanol molecules in low-temperature solids: a matrix isolation study. *Phys. Chem. Chem. Phys.* **2016**, *18* (47), 32503−32513.
(75) Zasimov, P. V.; Belousov, A. V.; Baranova, I. A.; Feldman, V. I. Quantitative assessment of the absorbed dose in cryodeposited noble-gas films under X-ray irradiation: Simulation vs. experiment. *Radiat. Phys. Chem.* **2020**, *177*, 109084.
(76) Weber, R. T. *WIN-EPR SIMFONIA manual*, Ver. 1.2; Bruker Instruments, Inc.: Billerica, MA, 1995.
(77) Stoll, S.; Schweiger, A. EasySpin, a comprehensive software package for spectral simulation and analysis in EPR. *J. Magn. Reson.* **2006**, *178* (1), 42−55.
(78) Barclay, A. J.; Mohandesi, A.; Michaelian, K. H.; McKellar, A. R. W.; Moazzen-Ahmadi, N. Infrared observation of OC−C_2H_2, OC−$(C_2H_2)_2$ and their isotopologues. *Mol. Phys.* **2018**, *116*, 3468−3474.
(79) Rupper, P.; Merkt, F. Intense narrow-bandwidth extreme ultraviolet laser system tunable up to 20 eV. *Rev. Sci. Instrum.* **2004**, *75*, 613−622.
(80) Erman, P.; Karawajczyk, A.; Rachlew-Kallne, E.; Stromholm, C.; Larrson, J.; Perrson, A.; Zerne, R. Direct determination of the ionization potential of CO by resonantly enhanced multiphoton ionization mass spectroscopy. *Chem. Phys. Lett.* **1993**, *215*, 173−178.
(81) Yuan, H.; Cremer, D. The expectation value of the spin operator S^2 as a diagnostic tool in coupled cluster theory: the advantages of using UHF-CCSD theory for the description of homolytic dissociation. *Chem. Phys. Lett.* **2000**, *324*, 389−402.
(82) Kitsaras, M.-P.; Stopkowitz, S. Spin contamination in MP2 and CC2, a surprising issue. *J. Chem. Phys.* **2021**, *154*, 131101.
(83) Lee, T. J.; Rice, J. E.; Schaefer, H. F., III The infrared spectrum of the acetylene radical cation $C_2H_2^+$. A theoretical study using SCF, MCSCF, and CI methods. *J. Chem. Phys.* **1987**, *86* (5), 3051−3053.
(84) Parshutkina, A. A.; Feldman, V. I. IR spectroscopic study of the intermediate products of low-temperature radiolysis of sulfur hexafluoride. *High. Energy Chem.* **2001**, *35*, 204−206.
(85) Kameneva, S. V.; Tyurin, D. A.; Feldman, V. I. Characterization of the HCN···CO complex and its radiation-induced transformation to HNC···CO in cold media: an experimental and theoretical investigation. *Phys. Chem. Chem. Phys.* **2017**, *19*, 24348−24356.
(86) Cochran, E. L.; Bowers, V. A.; Foner, S. N.; Jen, C. K. Multiple Trapping Sites for Hydrogen Atoms in Solid Argon. *Phys. Rev. Lett.* **1959**, *2* (2), 43−45.
(87) Tanskanen, H.; Khriachtchev, L.; Räsänen, M.; Feldman, V. I.; Sukhov, F. F.; Orlov, A. Y.; Tyurin, D. A. Infrared absorption and electron paramagnetic resonance studies of vinyl radical in noble-gas matrices. *J. Chem. Phys.* **2005**, *123* (6), 064318.
(88) Yamada, T.; Komaguchi, K.; Shiotani, M.; Benetis, N. P.; Sørnes, A. R. High-Resolution EPR and Quantum Effects on CH_3, CH_2D, CHD_2, and CD_3 Radicals under Argon Matrix Isolation Conditions. *J. Phys. Chem. A* **1999**, *103* (25), 4823−4829.
(89) Cochran, E. L.; Adrian, F. J.; Bowers, V. A. ESR study of ethynyl and vinyl free radicals. *J. Chem. Phys.* **1964**, *40* (1), 213−220.
(90) Graham, W. R. M.; Dismuke, K. I.; Weltner, W., Jr. C_2H radical: ^{13}C hyperfine interaction and optical spectrum. *J. Chem. Phys.* **1974**, *60* (10), 3817−3823.
(91) Kasai, P. H. Electron spin resonance studies of vinyl, propargyl, and butatrienyl radicals isolated in argon matrices. *J. Am. Chem. Soc.* **1972**, *94* (17), 5950−5956.
(92) Adrian, F. J.; Cochran, E. L.; Bowers, V. A. ESR spectrum and structure of the formyl radical. *J. Chem. Phys.* **1962**, *36* (6), 1661−1672.
(93) Ryazantsev, S. V.; Tyurin, D. A.; Feldman, V. I. Experimental determination of the absolute infrared absorption intensities of formyl radical HCO. *Spectrochim. Acta A Mol. Biomol.* **2017**, *187*, 39−42.
(94) Forney, D.; Jacox, M. E.; Thompson, W. E. The vibrational spectra of molecular ions isolated in solid neon: $HCCH^+$ and HCC^-. *J. Mol. Spectrosc.* **1992**, *153*, 680−691.
(95) Andrews, L.; Kushto, G. P.; Zhou, M.; Willson, S. P.; Souter, P. F. Infrared spectrum of CCH^+ in solid argon and neon. *J. Chem. Phys.* **1999**, *110*, 4457−4466.
(96) Toriyama, K.; Nunome, K.; Iwasaki, M. Structures and reactions of radical cations of some prototype alkanes in low temperature solids as studied by ESR spectroscopy. *J. Chem. Phys.* **1982**, *77*, 5891−5912.
(97) Feldman, V. I.; Sukhov, F.; Orlov, A.; Kadam, R.; Itagaki, Y.; Lund, A. Effect of matrix and substituent on the electronic structure of trapped benzene radical cations. *Phys. Chem. Chem. Phys.* **2000**, *2*, 29−35.
(98) Loomis, R. A.; McGuire, B. A.; Shingledecker, C.; Johnson, C. H.; Blair, S.; Robertson, A.; Remijan, A. J. Investigating the minimum energy principle in searches for new molecular species − The case of H_2C_3O isomers. *Astrophys. J.* **2015**, *799* (1), 34.
(99) Loison, J. C.; Agúndez, M.; Marcelino, N.; Wakelam, V.; Hickson, K. M.; Cernicharo, J.; Gerin, M.; Roueff, E.; Guélin, M. The interstellar chemistry of H_2C_3O isomers. *Mon. Not. R. Astron. Soc.* **2016**, *456*, 4101−4110.
(100) Shingledecker, C. N.; Álvarez-Barcia, S.; Korn, V. H.; Kästner, J. The Case of H_2C_3O Isomers, Revisited: Solving the Mystery of the Missing Propadienone. *Astrophys. J.* **2019**, *878*, 80.
(101) Hudson, R. L.; Gerakines, P. A. Propynal, an interstellar molecule with an exceptionally strong C≡C infrared band−laboratory infrared data and applications. *Mon. Not. R. Astron. Soc.* **2019**, *482*, 4009−4017.

https://doi.org/10.1021/jacs.2c00295
J. Am. Chem. Soc. 2022, 144, 8115−8128